Determination of optical constants of n- and p-type GaAs as a function of carrier concentration

Charles W. Dickerson^a, John H. McElearney^a, Kevin A. Grossklaus^a, Thomas E. Vandervelde*^a Department of Electrical and Computer Engineering, Tufts University, Medford, MA, USA 02155

ABSTRACT

Variable angle spectroscopic ellipsometry was used to determine the optical properties of n- and p-type GaAs over a doping range of 4.6×10^{16} to 9.3×10^{18} cm⁻³ and a spectral range of 190 nm to 30 μ m. Increased doping concentration was observed to have several distinct effects on the samples' optical properties: the band edge broadens and shifts to a higher energy; the E_1 and $(E_1 + \Delta_1)$ absorption peaks blur together; the E_2 absorption peak decreases; sub-bandgap, infrared absorption increases. Additionally, the doping effects are generally stronger for n-type than for p-type GaAs. These findings will help inform future design of optoelectronics.

Keywords: Gallium arsenide, ellipsometry, refractive index, optoelectronics, sub-bandgap

1. INTRODUCTION

Gallium arsenide (GaAs) is widely used in the fabrication of optoelectronic devices, including photovoltaics^{1,2}, photodetectors³⁻⁸, and lasers^{9,10}. These devices often implement heavily doped layers, at which point long-wavelength, sub-bandgap absorption becomes a concern¹¹. For example, in multi-junction photovoltaic cells with doped GaAs as a middle junction, high absorption can reduce cell efficiency¹². Similarly, photovoltaic contact layers must have a high carrier concentration to facilitate conduction with the contact metal while still allowing photons to pass into absorbing layers. As such, the optical properties of these doped layers are vital in accurately modeling and designing GaAs-based optoelectronic devices.

While the effect of doping on the optical properties of other semiconductors, like Si^{13} , has been reported, the effect in GaAs has not been thoroughly characterized. Previous work has shown the absorption of n-type GaAs between 0.85 and 25 μm as a function of carrier concentration¹⁴, up to 5.4×10^{18} cm⁻³. Similarly, the IR absorption (50 to 500 μm) of n-type GaAs with low doping concentrations (up to 1.5×10^{16} cm⁻³) has been characterized¹⁵. The refractive index and extinction coefficient for n-type (1.4-1.8×10¹⁸ cm⁻³) and p-type (3-3.5×10¹⁸ cm⁻³) GaAs have been studied over a spectral range of 12.5 to 50 μm as well¹⁶.

This study builds upon prior work by measuring the complex refractive index $(\langle n \rangle + i \langle k \rangle)$ of n- and p-type GaAs as a function of carrier concentration from 4.6×10^{16} to 9.3×10^{18} cm⁻³ and over a spectral range of 190 nm to 30 μ m. Samples were grown by molecular beam epitaxy (MBE) and characterized by variable angle spectroscopic ellipsometry (VASE). Results of this work will enable more accurate modeling and design of GaAs-based devices.

2. MATERIALS AND METHODS

2.1 Sample Growth

Samples were grown by solid-source, molecular beam epitaxy (MBE) on semi-insulating, (100) oriented GaAs substrates using a Veeco GENxplor chamber. Ga fluxes were supplied using a high-temperature effusion cell, with As supplied by a valved cracker cell. Elemental Si and Be were used as n- and p-type dopants sources, respectively, and were co-deposited during film growth.

Source fluxes were determined by measuring beam equivalent pressures (BEP) at start of day using a N₂ calibrated ion gauge. Reflection high energy electron diffraction (RHEED) was used to both monitor the sample surface during growth, as well as determine the GaAs growth rate via Ga RHEED intensity oscillations. RHEED was also used to find the V:III BEP ratio at the GaAs stoichiometric point by adjusting the As valve position and watching for the (2 x 4) to (4 x 2) surface

^{*}tvanderv@ece.tufts.edu

reconstruction swap. Growth surface temperature was monitored by a combination of band edge thermometry and optical pyrometry using a k-Space Associates BandiT spectrometer and a BASF Exactus pyrometer respectively.

For all samples, the GaAs substrate was heated under an As overpressure to ~615 °C to first desorb the protective epiready oxide. The sample was then cooled to the GaAs growth temperature of 580 °C. An initial 100 nm undoped GaAs buffer was grown to smooth out the surface, followed by 500 nm of doped GaAs. The Ga flux was chosen to maintain a 1.0 ML/s growth rate, while the As flux was set to give a V:III BEP ratio of ~30:1 - roughly twice the BEP ratio at the GaAs stoichiometric point – to ensure a Group-V rich environment. Dopant cell temperatures were adjusted between samples to vary carrier concentration.

2.2 Hall Effect Measurement

Extrinsic carrier concentration and majority carrier mobility were determined by van der Pauw and Hall Effect measurement using a Lake Shore Cryotonics Hall Effect System. Samples were cleaved into 8 mm square pieces with In contacts applied to each corner. Contacts were annealed locally at $550\,^{\circ}$ C for 15-20 seconds each in order to diffuse the In into the doped GaAs film and ensure low resistance. Samples were excited with currents ranging from $25\text{-}500\,\mu\text{A}$, depending on doping, in an applied magnetic field of $1.38\,\text{T}$.

2.3 Ellipsometry

Spectroscopic ellipsometry is a robust technique used to measure the optical properties of a sample and extract those of an individual layer. SE measures the change in polarization state of s- and p-polarized light after reflection off a sample. S- and p-polarized light will reflect off a sample differently, which lends insight on the material's optical properties. The complex ratio of the reflected signals (ρ), normalized to the known incident signals, can be written in terms of the phase difference (Δ) and the ratio of their normalized amplitudes ($tan(\Psi)$):

$$\rho = \frac{r_p}{r_s} = \frac{E_{r,p}/E_{i,p}}{E_{r,s}/E_{i,s}} = \tan(\Psi)e^{i\Delta}$$
 (1)

We define a pseudo-dielectric function, $\langle \varepsilon \rangle$, for the sample stack by treating it as a monolithic material, where ϕ is the incidence angle¹⁷:

$$\langle \varepsilon \rangle = \langle \varepsilon_1 \rangle + i \langle \varepsilon_2 \rangle = \sin(\phi)^2 \cdot \left[1 + \tan(\phi)^2 \cdot \left(\frac{1 - \rho}{1 + \rho} \right)^2 \right],$$
 (2)

A layer-by-layer model can be fit to the collected data, allowing the optical properties of a desired layer to be extracted, either as the dielectric function above or the complex refractive index via the following conversion:

$$\langle \varepsilon \rangle = \langle \tilde{n} \rangle^2 = (\langle n \rangle + i \langle k \rangle)^2$$
 (3)

The optical properties reported here were determined using two J.A. Woollam variable angle spectroscopic ellipsometers (VASE): a UV-VIS VASE spanning a spectral range of 0.19-2.65 μ m and an IR VASE covering the range of 1.7-30 μ m. Scans were taken with step sizes of 4 nm and 15 spectra/revolution, respectively. With both instruments, measurements were made at room temperature, at incident angles of 70° and 75°. For IR VASE measurements, the back side of each sample was roughened using a sand blaster to reduce long-wavelength back-surface reflections.

A three-layer model was employed to fit the ellipsometry data. This included an intrinsic GaAs substrate layer, a doped GaAs layer, and a surface oxide/roughness layer. The substrate layer used optical properties from the literature for the UV-VIS VASE¹⁸ and IR VASE¹⁹ models, and its thickness was fixed at 500 μ m. For the UV-VIS VASE models, the doped GaAs layer was built from numerous oscillators based on features common to the dielectric functions of semiconductors²⁰. IR VASE models utilized a combination of free carrier Drude and so-called TOLO²¹ models, while additional oscillators were required for the highly doped samples. The surface layer is a Bruggeman effective medium approximation, which is a 50/50 mix of the underlying doped GaAs layer and void. This approximation effectively models both surface roughness and oxides²². Parameters for the oscillator and free carrier models, in addition to the doped GaAs layer and surface layer thicknesses, were fit to the measured pseudo-dielectric function. The optical properties reported here were extracted from the doped GaAs layer as a function of wavelength.

3. RESULTS AND DISCUSSION

3.1 UV-VIS VASE

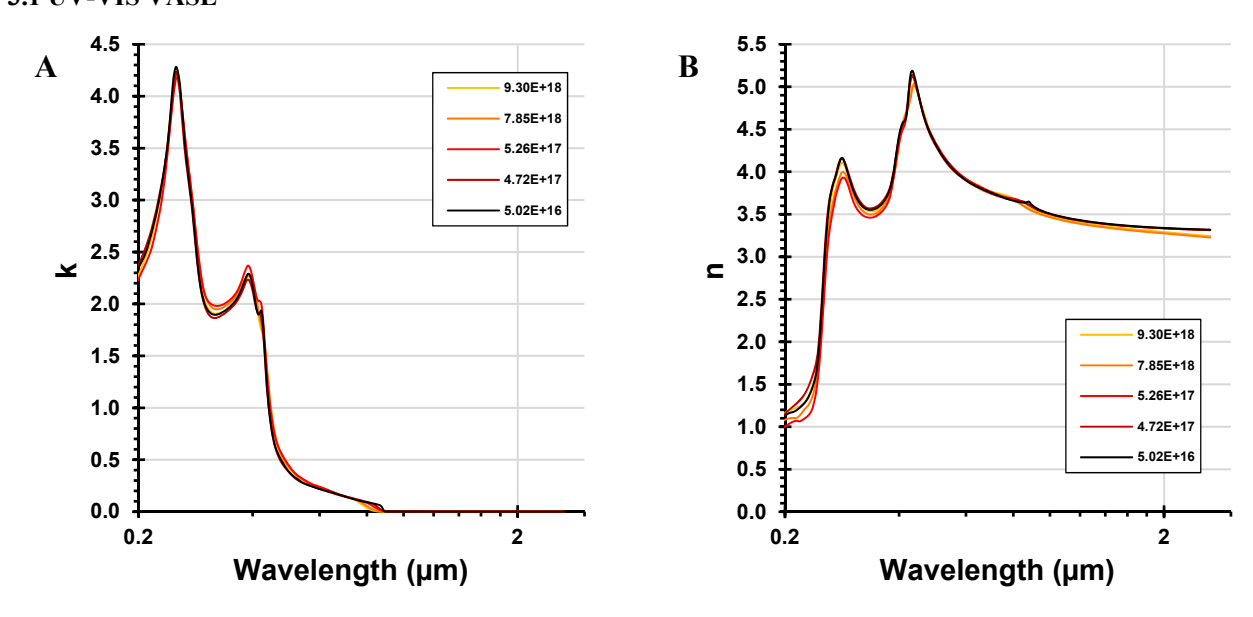


Figure 1. Extinction coefficient (A) and refractive index (B) of n-type GaAs at various carrier concentrations determined by UV-VIS VASE.

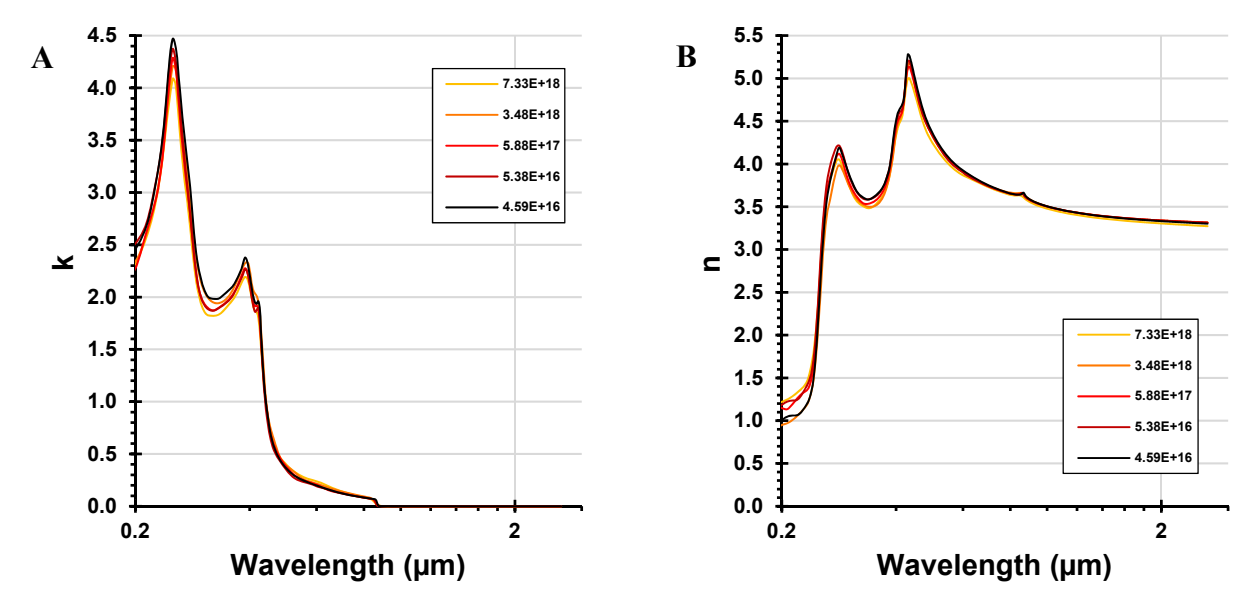


Figure 2. Extinction coefficient (A) and refractive index (B) of p-type GaAs at various carrier concentrations determined by UV-VIS VASE.

Figures 1 and 2 show the optical properties of the n- and p-type GaAs samples over the full spectrum covered by the UV-VIS VASE. As doping increases, certain trends become visible at key features on the spectrum; namely the band edge E_0 , the E_1 and $(E_1 + \Delta_1)$ peaks, and the E_2 peak. It has been shown previously that these critical points in the dielectric function can be correlated to specific transitions in the electronic band structure^{23,24}.

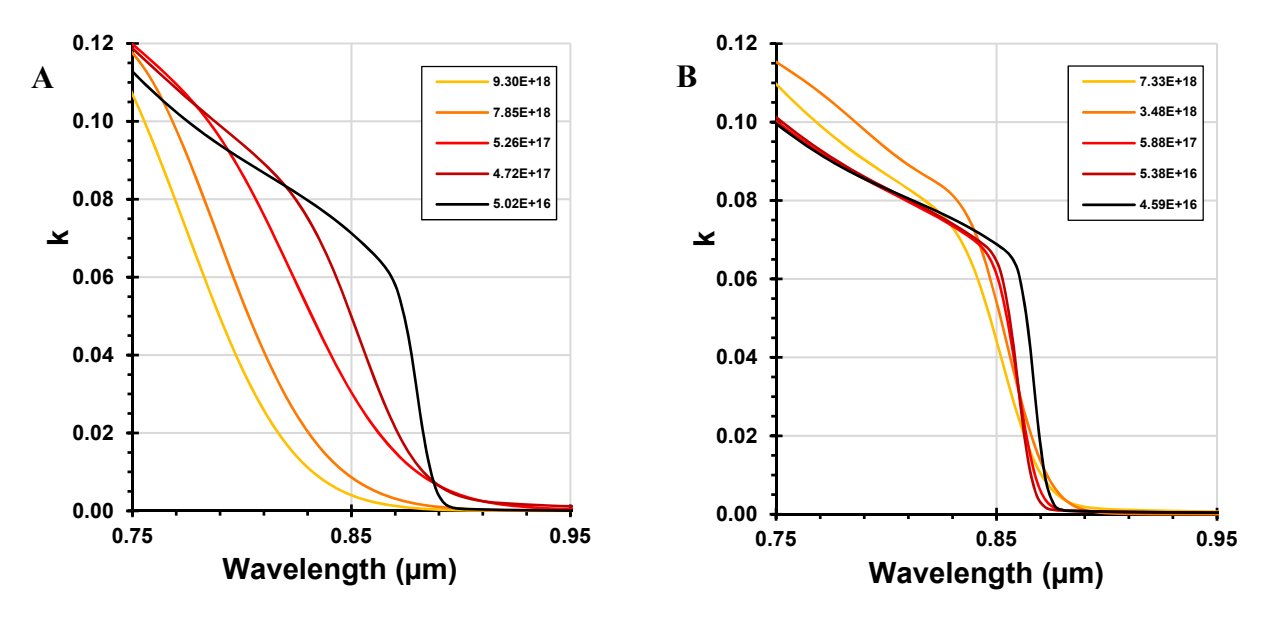


Figure 3. Extinction coefficient of n-type (A) and p-type (B) GaAs at the band edge, E₀.

At the band edge, E_0 , the effect of doping is similar in both n- and p-type GaAs: as doping increases, the band edge broadens and shifts to a higher energy. This effect has previously been observed for n-type $GaAs^{25,26}$ but others report the bandgap narrowing with increased doping²⁷. Bandgap shrinkage has also been observed p-type $GaAs^{28}$.

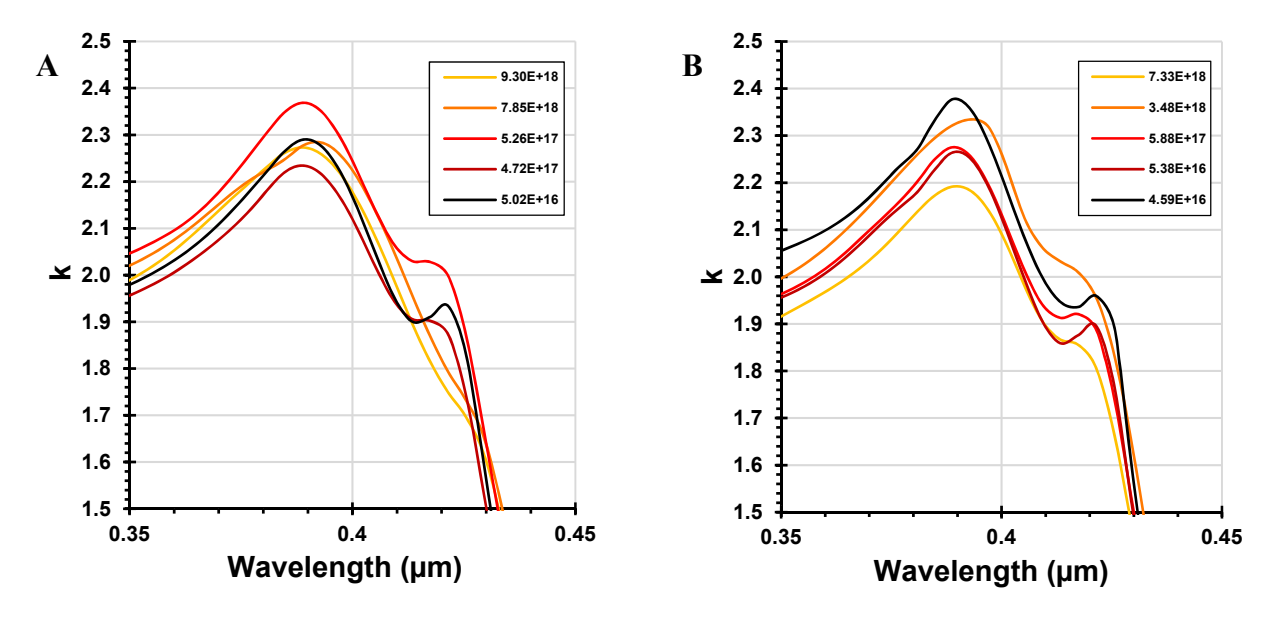


Figure 4. Extinction coefficient of n-type (A) and p-type (B) GaAs at the E_1 and $(E_1 + \Delta_1)$ peaks.

In both n-type and p-type materials, the E_1 and $(E_1 + \Delta_1)$ peaks – corresponding to band transitions to the conduction band from the valence and split-off bands at the Λ point, respectively – are distinct at low doping concentrations. As doping increases, the E_1 peak and its corresponding absorption mechanism are suppressed, blurring the features together.

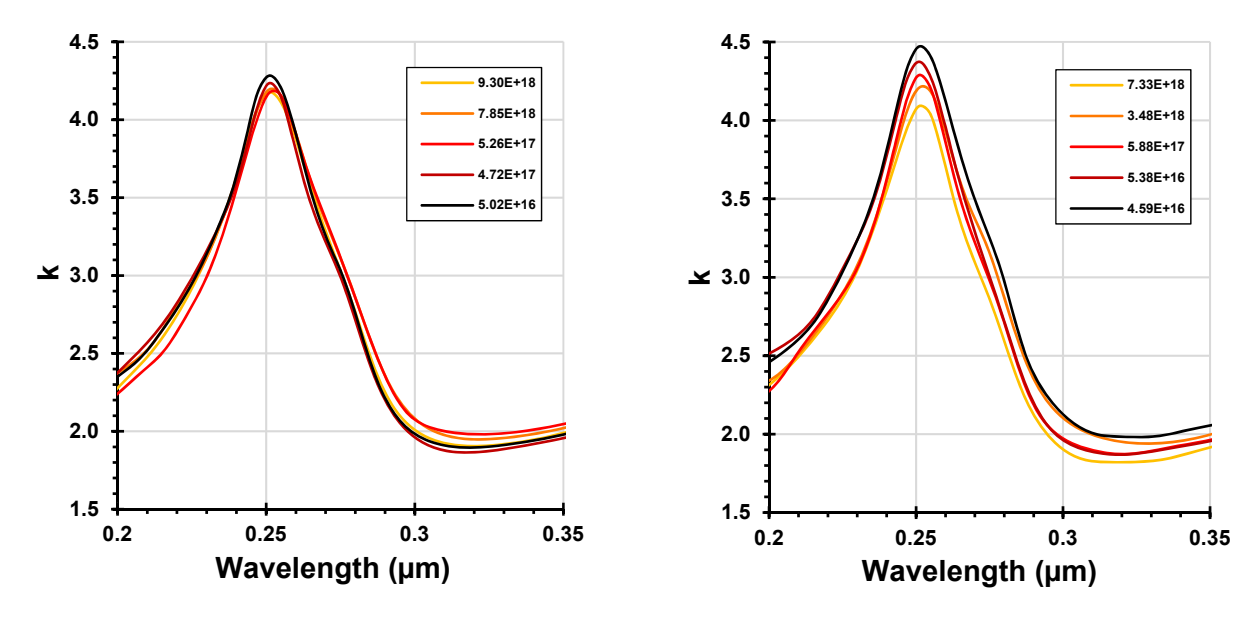


Figure 5. Extinction coefficient of n-type (A) and p-type GaAs (B) at the E2 peak.

Increasing doping tends to decrease the E_2 absorption peak, though the trend is clearer in p-type GaAs, which is also observed in Si^9 . It is important to note that the E_2 peak is highly sensitive to surface quality²⁹ (oxide layer, roughness, etc.) and could thus be the source of the inconsistent trend in the n-type material.

3.2 IR VASE

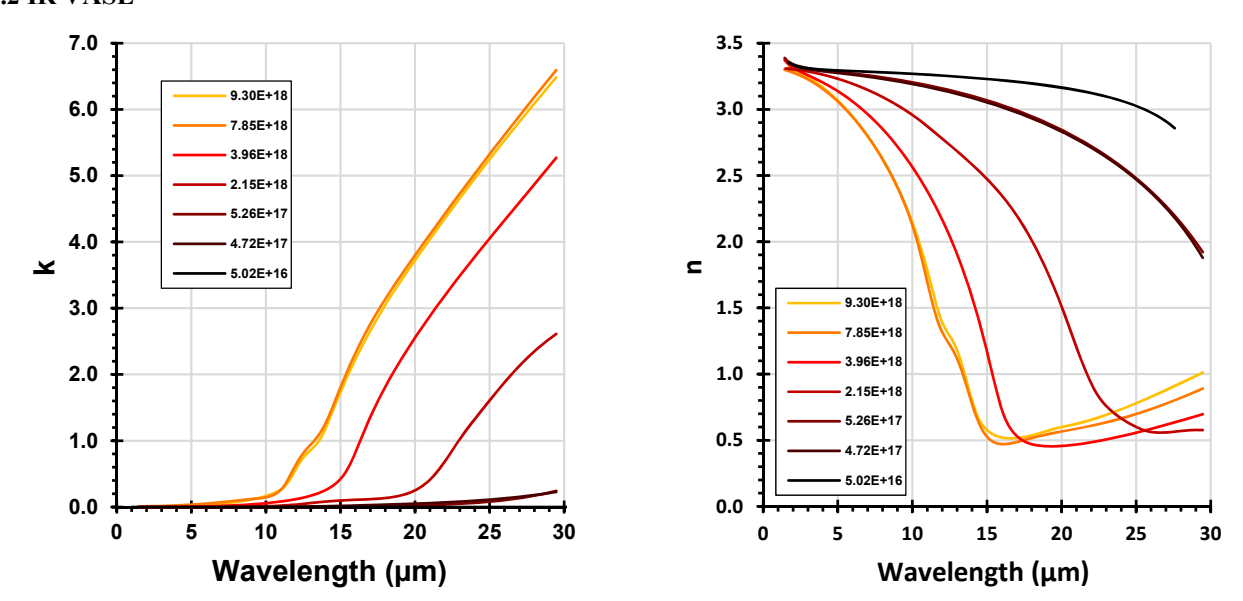
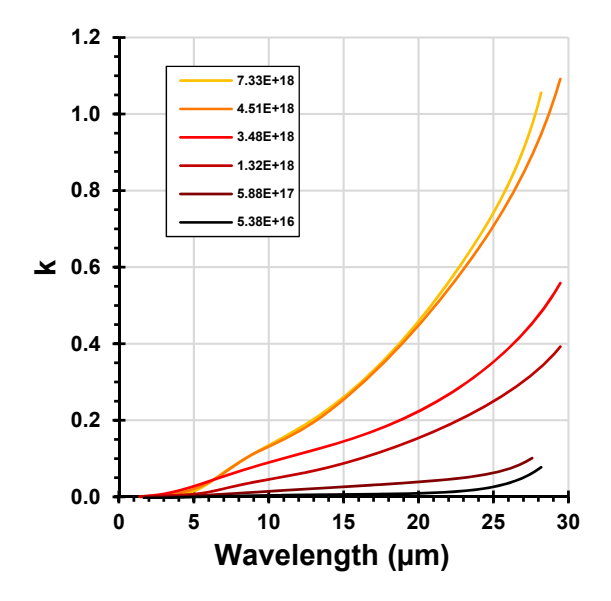


Figure 6. Extinction coefficient (A) and refractive index (B) of n-type GaAs at various carrier concentrations determined by IR VASE.



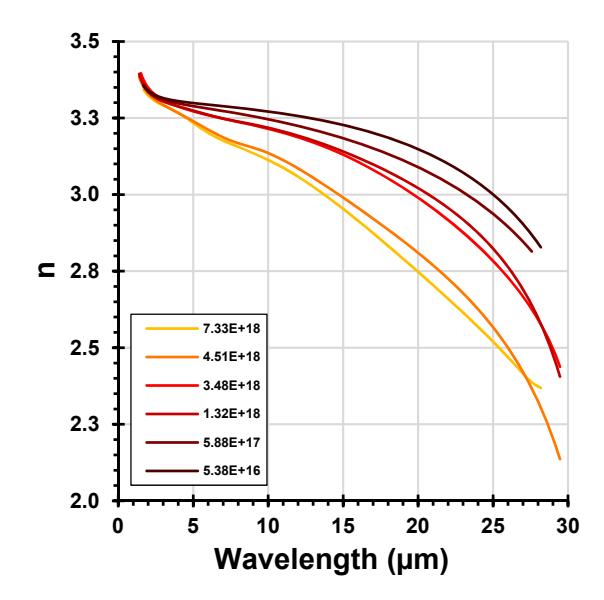


Figure 7. Extinction coefficient (A) and refractive index (B) of p-type GaAs at various carrier concentrations determined by IR VASE.

The extinction coefficients and refractive indices of n- and p-type GaAs in the infrared region are shown in Figs. 6 and 7. The data shows that increasing the doping concentration causes an increase in sub-bandgap absorption for both n- and p-type materials. For all samples, absorption increases at longer wavelengths. Across the measured IR range, absorption is significantly higher for the n-type samples, which could prove challenging for n-on-p optoelectronics with n-type top layers.

4. CONCLUSION

In this work, we determine the change in optical properties of n- and p-type GaAs due to doping, as determined by variable angle spectroscopic ellipsometry. Key observations in the UV/visible data include the broadening and shift of the band edge E_0 , the smearing of E_1 and $(E_1 + \Delta_1)$ peaks, and the decrease of the E_2 absorption peak with increasing doping. In the IR data, increasing the carrier concentration resulted in increased absorption, and the optical properties of n-type GaAs were affected by doping more strongly than p-type GaAs. The data we report here will aid in the modeling and design of GaAs-based optoelectronics with applications ranging from infrared to ultraviolet spectral regions.

5. ACKNOWLEDGEMENTS

This work is supported by the National Science Foundation (ECCS-2225641 and ECCS-2120568). Samples were grown in the Tufts Epitaxial Core Facility on equipment supported by NSF EECS 1337783.

6. SUPPLEMENTARY INFORMATION

https://doi.org/10.5281/zenodo.10632062

REFERENCES

[1] Dimroth, F., Grave, M., Beutel, P., Fiedeler, U., Karcher, C., Tibbits, T. N. D., Oliva, E., Siefer, G., Schachtner, M., Wekkeli, A., Bett, A. W., Krause, R., Piccin, M., Blanc, N., Drazek, C., Guiot, E., Ghyselen, B., Salvetat, T., Tauzin, A., et al., "Wafer bonded four-junction GaInP/GaAs//GaInAsP/GaInAs concentrator solar cells with 44.7% efficiency," Progress in Photovoltaics 22(3), 277–282 (2014).

- [2] Zayan, A., Stevens, M. and Vandervelde, T. E., "GaAsBi alloys for photovoltaic and thermophotovoltaic applications," 2016 IEEE 43rd Photovoltaic Specialists Conference (PVSC), 2839–2843, IEEE, Portland, OR, USA (2016).
- [3] Downs, C. and Vandervelde, T. E., "Progress in Infrared Photodetectors Since 2000," Sensors 13(4), 5054–5098 (2013).
- [4] Shao, J., Vandervelde, T. E., Barve, A., Jang, W.-Y., Stintz, A. and Krishna, S., "Enhanced normal incidence photocurrent in quantum dot infrared photodetectors," Journal of Vacuum Science & Technology B **29**(3), 03C123 (2011).
- [5] Vandervelde, T. E. and Krishna, S., "Progress and prospects for quantum dots in a well infrared photodetectors," Journal of Nanoscience Nanotechnology **10**(3), 1450–1460 (2010).
- [6] Cellek, O. O., Reno, J. L. and Zhang, Y.-H., "Optically addressed near and long-wave infrared multiband photodetectors," Applied Physics Letters **100**(24), 241103 (2012).
- [7] Chen, X., Wang, D., Wang, T., Yang, Z., Zou, X., Wang, P., Luo, W., Li, Q., Liao, L., Hu, W. and Wei, Z., "Enhanced Photoresponsivity of a GaAs Nanowire Metal-Semiconductor-Metal Photodetector by Adjusting the Fermi Level," ACS Appl. Mater. Interfaces 11(36), 33188–33193 (2019).
- [8] Smith, F. W., Le, H. Q., Diadiuk, V., Hollis, M. A., Calawa, A. R., Gupta, S., Frankel, M., Dykaar, D. R., Mourou, G. A. and Hsiang, T. Y., "Picosecond GaAs-based photoconductive optoelectronic detectors," Applied Physics Letters 54(10), 890–892 (1989).
- [9] Schnitzer, I., Yablonovitch, E., Caneau, C. and Gmitter, T. J., "Ultrahigh spontaneous emission quantum efficiency, 99.7% internally and 72% externally, from AlGaAs/GaAs/AlGaAs double heterostructures," Applied Physics Letters 62(2), 131–133 (1993).
- [10] Qu, Y., Yuan, S., Liu, C. Y., Bo, B., Liu, G. and Jiang, H., "High-Power InAlGaAs/GaAs and AlGaAs/GaAs Semiconductor Laser Arrays Emitting at 808 nm," IEEE Photon. Technol. Lett. 16(2), 389–391 (2004).
- [11] Vest, B., Fix, B., Jaeck, J. and Haïdar, R., "Competition between sub-bandgap linear detection and degenerate two-photon absorption in gallium arsenide photodiodes," J. Eur. Opt. Soc.-Rapid Publ. 12(1), 26 (2016).
- [12] Omelchenko, S. T., Wong, J., Lewis, N. S. and Atwater, H. A., "Effects of Sub-gap Absorption on Photovoltaic Performance," 2018 IEEE 7th World Conference on Photovoltaic Energy Conversion (WCPEC) (A Joint Conference of 45th IEEE PVSC, 28th PVSEC & 34th EU PVSEC), IEEE, 1837–1840 (2018).
- [13] Viña, L. and Cardona, M., "Effect of heavy doping on the optical properties and the band structure of silicon," Phys. Rev. B **29**(12), 6739–6751 (1984).
- [14] Spitzer, W. G. and Whelan, J. M., "Infrared Absorption and Electron Effective Mass in n-Type Gallium Arsenide," Phys. Rev. 114(1), 59–63 (1959).
- [15] Perkowitz, S., "Far infrared free-carrier absorption in n-type gallium arsenide," Journal of Physics and Chemistry of Solids **32**, 2267-2274 (1971).
- [16] Engelbrecht, J. A. A., Lee, I. G. and Venter, D. J. L., "Optical characterization of doped and undoped GaAs at 300 K," Infrared Physics **27**(1), 57–62 (1987).
- [17] Woollam, J. A., Johs, B. D., Herzinger, C. M., Hilfiker, J. N., Synowicki, R. A. and Bungay, C. L., "Overview of variable-angle spectroscopic ellipsometry (VASE): I. Basic theory and typical applications," Proc. SPIE 10294, Optical Metrology: A Critical Review, 1029402 (1999).
- [18] Data accessed through WVASE Material Library. Collected at University of Nebraska-Lincoln by J. A. Woollam.
- [19] Palik, E. D. and Ghosh, G., eds., "Handbook of optical constants of solids", Academic Press, San Diego, 429-443 (1998).
- [20] Erman, M., Theeten, J. B., Chambon, P., Kelso, S. M. and Aspnes, D. E., "Optical properties and damage analysis of GaAs single crystals partly amorphized by ion implantation," Journal of Applied Physics **56**(10), 2664–2671 (1984).
- [21] Kirk, C. T., "Quantitative analysis of the effect of disorder-induced mode coupling on infrared absorption in silica," Phys. Rev. B **38**(2), 1255–1273 (1988).
- [22] Tompkins, H. G. and Irene, E. A., eds., "Handbook of ellipsometry", William Andrew Pub.; Springer, Norwich, NY: Heidelberg, Germany, 261 (2005).
- [23] Chelikowsky, J. R. and Cohen, M. L., "Erratum: Nonlocal pseudopotential calculations for the electronic structure of eleven diamond and zinc-blende semiconductors," Phys. Rev. B **30**(8), 4828–4828 (1984).
- [24] Lautenschlager, P., Garriga, M., Logothetidis, S. and Cardona, M., "Interband critical points of GaAs and their temperature dependence," Phys. Rev. B **35**(17), 9174–9189 (1987).

- [25] Borghs, G., Bhattacharyya, K., Deneffe, K., Van Mieghem, P. and Mertens, R., "Band-gap narrowing in highly doped *n*-and *p*-type GaAs studied by photoluminescence spectroscopy," Journal of Applied Physics **66**(9), 4381–4386 (1989).
- [26] Lideikis, T. and Treideris, G., "Near band-gap photoluminescence of the MOCVD-grown heavily Si-doped GaAs," Semicond. Sci. Technol. **4**(11), 938–942 (1989).
- [27] Luo, H. T., Shen, W. Z., Zhang, Y. H. and Yang, H. F., "Study of band gap narrowing effect in n-GaAs for the application of far-infrared detection," Physica B: Condensed Matter **324**(1–4), 379–386 (2002).
- [28] Harmon, E. S., Melloch, M. R. and Lundstrom, M. S., "Effective band-gap shrinkage in GaAs," Applied Physics Letters 64(4), 502–504 (1994).
- [29] Mahtab, M., Synowicki, R., Bahrami-Yekta, V., Bannow, L. C., Koch, S. W., Lewis, R. B. and Tiedje, T., "Complex dielectric function of GaAs_{1-x}Bi_x as a function of Bi content," Phys. Rev. Materials **3**(5), 054601 (2019).